Draft version February 12, 2022
Typeset using LaTeX **preprint** style in AASTeX62

arXiv:1909.05574v1 [astro-ph.SR] 12 Sep 2019

Spectropolarimetry of the Solar Mg II h and k Lines

R. Manso Sainz,[1] T. del Pino Alemán,[2] R. Casini,[3] and S. McIntosh[3]

[1] *Max-Planck-Institut für Sonnensystemforschung*
Justuts-von-Liebig-Weg 3, 37077
Göttingen, Germany
[2] *Instituto de Astrofísica de Canarias*
Av. Vía Láctea s/n, 38205
La Laguna, Tenerife, Spain
[3] *High Altitude Observatory, National Center for Atmospheric Research*
PO-Box 3000, Boulder, CO 80307-3000, USA

(Received July 31, 2019; Revised September 2, 2019; Accepted September 3, 2019)

Submitted to ApJ

ABSTRACT

We report on spectropolarimetric observations across the Mg II h and k-lines at 2800 Å made by the Ultraviolet Spectrometer and Polarimeter onboard the Solar Maximum Mission satellite. Our analysis confirms the strong linear polarization in the wings of both lines observed near the limb, as previously reported, but also demonstrates the presence of a negatively (i.e., radially oriented) polarized signal between the two lines. We find evidence for fluctuations of the polarization pattern over a broad spectral range, resulting in some depolarization with respect to the pure scattering case when observed at very low spatial and temporal resolutions. This is consistent with recent theoretical modeling that predicts this to be the result of redistribution effects, quantum interference between the atomic levels of the upper term, and magneto-optical effects. A first attempt at a quantitative exploitation of these signals for the diagnosis of magnetic fields in the chromosphere is attempted. In active regions, we present observations of circular polarization dominated by the Zeeman effect. We are able to constrain the magnetic field strength in the upper active chromosphere using an analysis based on the magnetograph formula, as justified by theoretical modeling. We inferred a significantly strong magnetic field ($\sim 500\,\mathrm{G}$) at the $2.5\,\sigma$ level on an exceptionally active, flaring region.

Keywords: Spectropolarimetry — UV — Solar chromosphere — Solar magnetic fields

1. INTRODUCTION

The Ultraviolet Spectrometer and Polarimeter (UVSP; Calvert et al. 1979; Woodgate et al. 1980), on board the *Solar Maximum Mission* (SMM; Bohlin et al. 1980; Strong et al. 1999) provided the first successful opportunity to investigate the Sun through ultraviolet (UV) spectropolarimetry. Observations in the UV allow access to the highest and more energetic regions of the solar chromosphere

and transition region (TR); polarimetry of spectral lines in that spectral window offer the possibility of probing the magnetic field and the highly anisotropic, dynamic processes taking place in these regions. Observations of the Zeeman effect in the C IV 1548 Å line have in fact been used to measure the magnetic field in the TR over active regions (ARs; Tandberg-Hanssen et al. 1981; Henze et al. 1982; Hagyard et al. 1983). Linear polarization in the S I 1437 Å line, most likely due to impact by beamed electrons, provided important insights into how flares work and the dynamics of these high layers (Henoux et al. 1983).

The Mg II UV doublet at ∼2800 Å (h and k lines) was observed using full Stokes polarimetry in quiet regions near the solar limb in search of scattering polarization (Henze & Stenflo 1987). Here, we present a reanalysis of those observations. The motivation for doing so stems from recent theoretical findings about the formation of broadband polarization in the Mg II UV doublet. Based on a thorough theoretical and modeling analysis, del Pino Alemán et al. (2016) predicted that a very broad spectral region ∼30 Å around the h and k lines should be highly linearly polarized and, surprisingly, modulated by the chromospheric magnetic field via magneto-optical (M-O) effects. We also analyze observations in ARs that appear to be dominated by the Zeeman effect. del Pino Alemán et al. (2016) and Alsina Ballester et al. (2016) have found that despite the complexity of the spectroscopic and transfer mechanisms involved in their formation, the circular polarization in the core of the lines satisfies the magnetograph formula. These findings have potentially important observational consequences. The former opens the interesting possibility of broadband filter polarimetry in the UV; the latter justifies a simplified approach to the magnetometry in these highly complex layers of the Sun.

2. OBSERVATIONS

The observations were made with SMM/UVSP in 1980 March-April (Table 1), and 1984 October. UVSP consisted of a Gregorian telescope, a spectrograph (Ebert-Fastie configuration), and a rotating MgF_2 waveplate that could be inserted in the light path, acting as the polarization modulator, while the grating itself served as the polarization analyzer.

The detector was a single photocathode. Spectral scans were made by rotating the grating of the spectrometer. For each given wavelength and spatial position, a full polarimetric modulation cycle (consisting of 16 steps) was performed before changing to a different wavelength or position.

A detailed description of the demodulation scheme and analysis of the observations is given in the Appendix. Most of the analysis follows standard techniques (e.g., Woodgate et al. 1980; Tandberg-Hanssen et al. 1981; Henoux et al. 1983; Henze & Stenflo 1987); we present it here for completeness and to justify the particularities of our approach. We improve upon previous analyses on three different aspects: recalibration of the linear polarization, analysis of the circular polarization, and a careful, direct treatment of the error budget necessary for the statistical interpretation of the results.

2.1. *Limb and Disk-center Observations*

The observations were carried out at different wavelengths (up to 10, spanning 15 Å through the Mg II h & k doublet), with an entrance slit of 1″×180″, parallel to the solar limb, and an exit slit 0.02 Å wide. At each wavelength, the sun was rastered perpendicularly to the slit seven times at 10″before moving to a new wavelength. A complete modulation cycle lasted 40 s (16 × 2.5 s), and the full spatial raster at a given wavelength ∼ 5 minutes.

The observational strategy was optimal for detecting linear (scattering) polarization at the 10 selected wavelength positions in the wings (two blueward of the k-line, three redward of the h-line)

and between the lines (five). With the modulation scheme of UVSP, linear polarization (Stokes-Q and U) appears at higher frequencies than circular polarization. Slow monotonic intensity drifts have more power at lower frequencies and may affect severely circular polarization signals, while linear polarization, at higher frequencies, is more protected from intensity-to-polarization cross-talk. In the longer exposures used for scattering at the limb, circular polarization was often vulnerable to such effects and those data rejected. A more detailed discussion can be found in the Appendix. The remaining reliable circular polarization observations (not shown in Fig. 1) were compatible with null signal, as expected.

Observations at disk center were taken with the same instrumental configuration and observational strategy as for the limb observations, which allowed us to calibrate for spurious instrumental polarization (Manso Sainz et al. 2017)— a common strategy for inflight calibration even in modern spectropolarimeters (e.g., Giono et al. 2017). Averaging over all the slit positions and wavelengths, we find negligible amounts of circular polarization and Stokes U, but a residual signal $Q/I \sim 0.005$ (see Appendix). All the observations reported here have been recalibrated to this Q/I "zero level". This step, not taken by Henze & Stenflo (1987), has important consequences for our confirmation of their tentative detection.

A scan along the whole range lasted up to ∼50 min, far longer than the typical dynamic timescales in the chromosphere and TR, thus precluding the reconstruction of resolved profiles. Since the wavelength positions are reported in the logbooks (Henze 1993) with very low accuracy, we adopted instead the values of Henze & Stenflo (1987).

2.2. *Active Region Observations*

A different strategy was followed to observe two ARs at two different positions on the solar disk, at two different times (Table 1). The aim here was to scan the core and nearby wings where the Zeeman polarization peaks appear. The profile of the Mg II k-line was scanned with a fixed spectral resolution of $\Delta\lambda \sim 100$ mÅ, at a fixed spatial position. The entrance slit was $3'' \times 3''$. This was done twice, consecutively.

The integration time per wavelength was much shorter: a modulation cycle lasted 16 s (16×1 s). This was enough to significantly reduce the number of observations severely affected by intensity drifts and also made it possible to reconstruct the line profile reliably (see Sect. 4 below). The total duration of the whole observation was $\sim 2 \times 12$ minutes. Table 1 summarizes the log record.

The demodulation and error analyses were otherwise performed as indicated in the Appendix.

3. LINEAR POLARIZATION IN THE WINGS: SCATTERING AT THE LIMB

Observations close to the limb were carried out motivated by theoretical calculations predicting very high polarization levels due to scattering in the wings of the Mg II doublet, and a significative negative polarization lobe between the h and k lines (Auer et al. 1980). The results were deemed only partially successful; a polarization increase toward the far wings was indeed clearly detected but the negative lobe could not be confidently confirmed (Henze & Stenflo 1987).

Our reanalysis definitely confirms the presence of the negative polarization lobe (Figure 1). By contrast, we find a lower degree of polarization in the wings—slightly below, in fact, than what would be expected in the absence of magnetic fields (pure scattering case). However, this is precisely consistent with the recent theoretical finding on the magnetic modulation of the broadband polarization pattern around the Mg II UV doublet due to M-O effects in the far wings (del Pino Alemán et al.

Table 1. AR observation log and inferred magnetic field

Exp.[a]	AR id NOAA	R[b]	Date	B[c] (σ) (G)	
00948	2363	0.5	31.03.80	120 (200)	69 (200)
01042		0.77	03.04.80	331 (200)	308 (200)
01182	2372	0.36	07.04.80	10 (100)	121 (100)
01237		0.08	09.04.80	516 (200)	158 (100)

[a]UVSP experiment number

[b]Radius vector from disk center ($R = 0$) to limb ($R = 1$).

[c]Magnetic field (in G) and 1σ uncertainty (between parenthesis) for each two consecutive modulations in a given experiment.

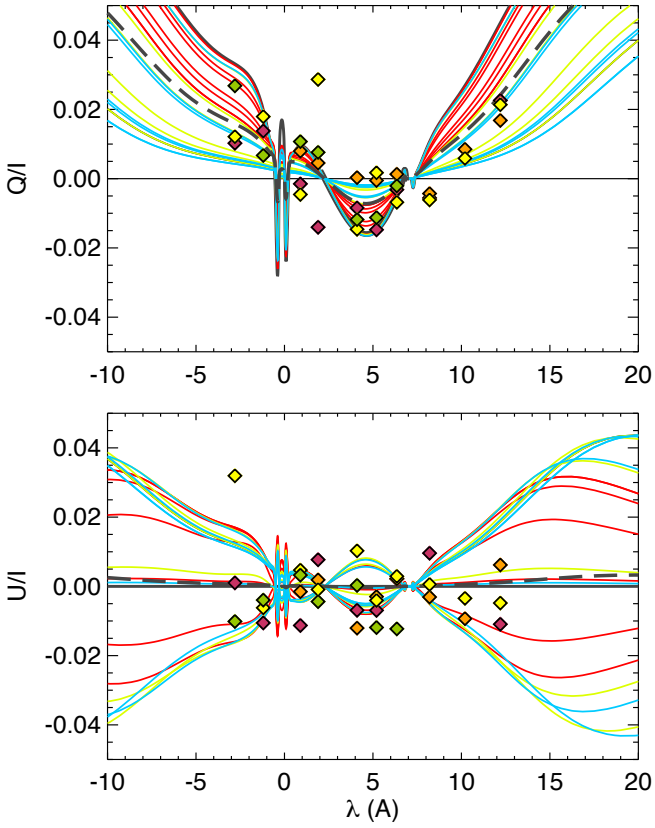


Figure 1. Polarization observed at the limb ($\mu = 0.15$). The symbols in four different colors correspond to four sets of observations performed on the 9th (2), 1984 October 19th and 20th. The scanning of a given "profile" required between 35 and 50 minutes. Solid lines illustrate the range of variability of the polarization pattern for different magnetic field configurations (red: $B = 20$ G, inclined $\theta_B = 60°$ with respect to the local vertical; yellow: $B = 50$ G, $\theta_B = 60°$; blue: $B = 50$ G, $\theta_B = 90°$; several different azimuths for each B and θ_B are shown). Dashed line: random azimuth field ($B = 50$ G, $\theta_B = 45°$). The thick dark line: polarization corresponding to the nonmagnetic, pure scattering case. The theoretical calculations are described in del Pino Alemán et al. (2016); Manso Sainz et al. (2017).

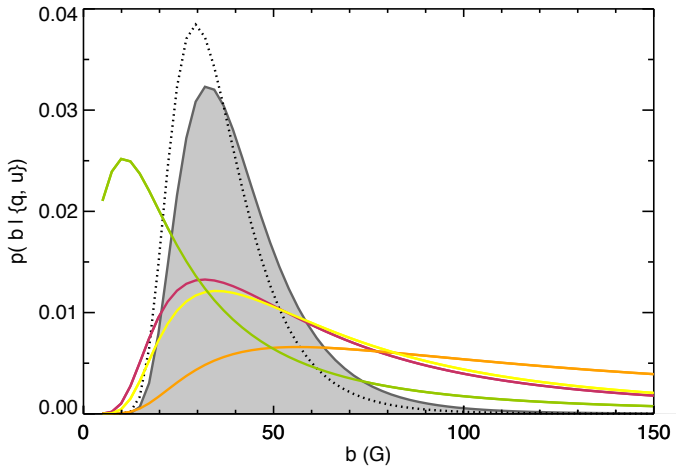


Figure 2. Posterior of the hyper-parameter b characterizing the Maxwellian distribution of fields adopted for the individual observations. Each color corresponds to a data set in Fig. 1. A joint analysis assumed the same Maxwellian distribution for all the observations and a uniform prior (shaded area) or Jeffreys prior (dotted) for b. A Maxwellian distribution with $b \approx 30\,\mathrm{G}$ is preferred as MAP, which has an average field of $B \approx 50\,\mathrm{G}$.

2016; Manso Sainz et al. 2017). Figure 1 shows that the observed fractional polarizations $q = Q/I$ and $u = U/I$ (previously unreported), fall nicely within the range of values allowed in a magnetized atmosphere: $|q|$ below the the pure scattering case, $|u| \geqslant 0$.

The spectropolarimetric pattern in a spectral region ± 20 Å around the Mg II UV doublet has been studied by del Pino Alemán et al. (2016) in great generality. Their modeling includes all the relevant spectroscopic and polarigenic mechanisms involved in the formation of the observed patterns—in particular, partial frequency redistribution (PRD), quantum coherence among the levels of the upper term ^2P, and, crucially, M-O effects. The calculations presented here were made for a semiempirical model atmosphere of the quiet sun (model C of Fontenla et al. 1993), for a grid of magnetic fields up to 1500 G, constant with height, different inclinations and azimuths with respect to the line of sight (LOS). Further details on the numerical methods, the code, and a detailed discussion on the physical processes involved can be found in del Pino Alemán et al. (2016); Casini et al. (2017).

It is not possible to uniquely determine the full magnetic field vector, $\boldsymbol{B}$, from just two observables, q and u. One may, however, infer information on a single parameter—say, the magnetic field strength, B—probabilistically with high confidence, by considering all the possibilities compatible with the observations (within uncertainties) and their probabilities, and marginalizing over all other less interesting (or uncertain) "noise" parameters. This Bayesian approach is the most natural and optimal way to extract the magnetic information from the data.

The observations at the limb were performed with very low (or none) spatial and temporal resolution, and they do not resolve the characteristic spatio-temporal dynamical evolution of the magnetic field on the chromosphere. So they have little information on the magnetic field vector configuration. The simplest model to describe this scenario is a macroscopically random azimuth magnetic field (in the local reference frame). Indeed, we expect the azimuth of the magnetic field to change much more widely during an observation than the inclination and polarity of the field. The synthetic averaged polarization profiles $\bar{q}$ and $\bar{u}$ depend on the magnetic field strength B and inclination θ_B, but we will

marginalize over θ_B at the end of the calculation.[1] This is a very simplified minimal model of the observations, yet it will allow a quantitative estimate of the magnetic field in the chromosphere.

For simplicity, we compare observations directly with the results of the numerical synthesis. Considering a finite spectral resolution does not noticeably affect the results due to the sparse sampling in wavelength and because the profiles are spectrally smooth in the wings. The relatively large uncertainties on the observations (wavelength position) are already compatible with neglecting these effects. This, however, would not be the case for high resolution spectral and spatial observations.

For a given set of observations $\{q_\ell, u_\ell\}$, $\ell = 1, \ldots, N_\ell$, assuming statistical independence among the N_ℓ wavelengths and Gaussian noise, we build a likelihood function $\mathcal{L}(B, \theta_B) \equiv p(\{q_\ell, u_\ell\}|B, \theta_B) = \mathrm{e}^{-\chi^2}/Z$, with merit function

$$\chi^2 = \sum_\ell \frac{[q_\ell - \bar{q}_\ell(B, \theta_B)]^2 + [u_\ell - \bar{u}_\ell(B, \theta_B)]^2}{2\sigma_\ell^2} \,, \tag{1}$$

and normalization constant $Z = (2\pi)^{N_\ell/2} \prod_\ell \sigma_\ell$, where $\bar{q}_\ell(B, \theta_B)$ and $\bar{u}_\ell(B, \theta_B)$ are calculated numerically, and $\sigma_\ell^2 \equiv \sigma^2(q_\ell) = \sigma^2(u_\ell) \approx \sigma^2(Q)/I = \sigma^2(U)/I$, is calculated as described in the Appendix. Assuming minimal *a priori* information on the magnetic field inclination, (e.g., isotropy), we marginalize over θ_B to obtain $\mathcal{L}(B) = \int \mathcal{L}(B, \theta_B)\, d\cos\theta_B$. The maximum-likelihood estimates for the four sets of observations are 20, 48, 50, and 70 G.

We may improve this estimate using the Bayes theorem and a simple hierarchical scheme assuming that the measured value B stems from a population with a Maxwellian distribution, $B \sim \mathcal{M}(b)$. The parameter b ($= \sqrt{\pi/8}$ times the mean of the distribution), will act as a hyper-parameter. The posterior for b is then $p(b|\{q_\ell, u_\ell\}) \propto \int \mathcal{L}(B) p(B|b) p(b)\, dB$; it is shown in Fig. 2, calculated for each of the four sets of observations.

Finally, we may pool all the observations assuming a common underlying distribution (hence, the same b) for all of them. We find a maximum *a posteriori* (MAP) for b of 29 G using an uninformative improper Jeffreys prior $p(b) = 1/b$ (e.g., Jaynes 2003), or 32 G for a uniform prior (see Fig. 2). This is corresponds to an average field $B \approx 46$ G.

4. CIRCULAR POLARIZATION IN THE LINE CORE: ZEEMAN EFFECT IN ACTIVE REGIONS

A simple, direct estimate of the magnetic field along the LOS, $B_\parallel$, is obtained from the observed intensity and circular polarization in a line profile, using the simple relation (Landi Degl'Innocenti & Landi Degl'Innocenti 1972)

$$V_\lambda = -C B_\parallel \frac{dI_\lambda}{d\lambda} \,, \tag{2}$$

where $C = \lambda_0^2\, g_{\rm eff}\, e/(4\pi mc^2) \approx 4.6686 \times 10^{-10} (\lambda_0/\text{Å})^2\, g_{\rm eff}$ mÅ G^{-1} (here symbols have their conventional meaning, and $g_{\rm eff}$ is the effective Landé factor). In our case, $\lambda_0 = 2795$ Å, and $g_{\rm eff} = 7/6$. The *magnetograph formula* (2) is valid in the weak magnetic field limit, but it is a good approximation in the core of the Mg II k-line for the magnetic field strengths expected in the upper solar chromosphere (del Pino Alemán et al. 2016; Alsina Ballester et al. 2016).

[1] Alternatively, including explicitly both the azimuth χ_B and inclination θ_B in the model $[q(B, \theta_B, \chi_B), u(B, \theta_B, \chi_B)]$, and then marginalizing over both parameters, would correspond to the case in which the magnetic field is (mostly) resolved in each individual observation and then combined *a posteriori* to statistically constrain the field. This is different from our case. Our observations do not resolve the magnetic geometry; we keep θ_B as the minimal parameter for marginalization to describe some degree of resolution.

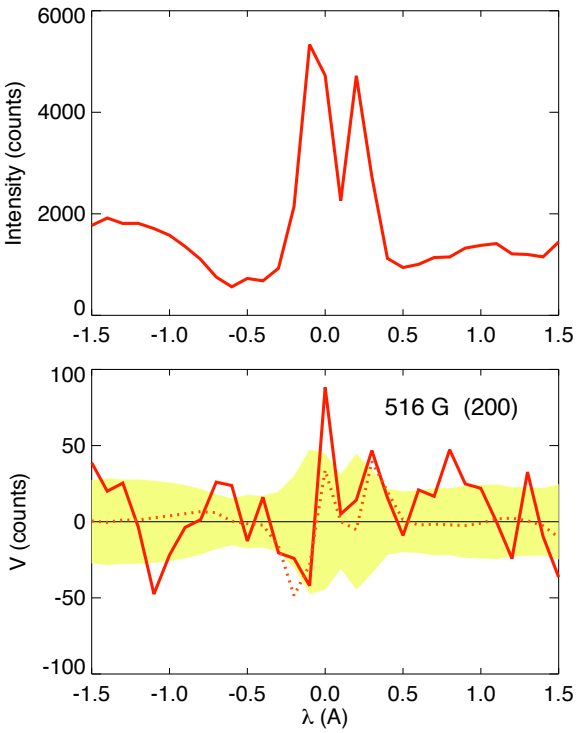


Figure 3. Intensity (upper panel) and circular polarization (lower panel) of the Mg II k-line observed in active region NOAA 2372 at the center of the solar disk (see entry for Exp. 01237 in Table 1). The yellow shaded area in the lower panel represents the $\sigma(V)$ level. The dotted line shows the fitting of the spectral derivative of the intensity to V. A magnetic field of 516 G ($\sigma(B) = 200$ G) is inferred according to the magnetograph formula.

Applying a maximum-likelihood argument to Eq. (2), we find an estimate for the longitudinal magnetic field and its uncertainty (Martínez González et al. 2012),

$$B_{\parallel} = -\frac{1}{C}\frac{\sum_l V_l I'_l/\sigma^2(V_l)}{\sum_l (I'_l)^2/\sigma^2(V_l)}\,, \tag{3a}$$

$$\sigma^2(B) = \frac{1}{C^2}\frac{1}{\sum_l (I'_l)^2/\sigma^2(V_l)}\,, \tag{3b}$$

where the derivative $I' = dI/d\lambda$ is calculated numerically. Noise at each wavelength is explicitly taken into account in Eqs. (3), which is particularly important for emission lines like this.

The values of the magnetic field inferred by applying Eqs. (3) to the eight UVSP observations of two ARs are tabulated in Table 1. In all but one case, there is no magnetic field detection above the the 2σ level. The observation of NOAA 2372 at disk center however, reaches 516 G at a 2.5 σ level (Fig. 3). Interestingly, NOAA 2372 was an exceptionally energetic AR during Solar Cycle 21, consisting of two large opposite polarity sunspots with a smaller bipole between them. It was reported flaring more than 50 times during its transit over the disk (Sawyer 1982; Machado et al. 1983; Ambastha & Bhatnagar 1988), and it showed an unusual evolution of the magnetic field in the photosphere (Krall et al. 1982; Rabin et al. 1984). Both factors—the favorable disk center geometry and the exceptionally strong activity—make it plausible that a magnetic field as high as 500 G was present at some point in the high chromospheric layers probed by the core of the Mg II k line.

5. DISCUSSION

Our reanalysis of the linear polarization in the wings of the Mg II h and k lines observed close to the solar limb confirms the presence of large (positive) signal in the outer wings and a negative polarization between the two lines. This conclusion differs from a previous analysis by Henze & Stenflo (1987), both quantitatively (they found an even larger polarization degree in the wings) and qualitatively (they found their results compatible with virtually no polarization between the two lines). Such discrepancy is resolved by our recalibration of the linear polarization. This reveals clearly the presence of the negative lobe, while at the same time it shows linear polarization in the wings that are below the theoretical zero-field level. This last result is explained as a combination of M-O effects in the wings (del Pino Alemán et al. 2016; Manso Sainz et al. 2017) and a lack of adequate spatio-temporal resolution. A simple statistical analysis suggests a magnetic field $B \approx 50\,\mathrm{G}$ in the region between ∼500-700 km of height where the observed line wings form (del Pino Alemán et al., submitted).

The analysis of the circular polarization produced by the Zeeman effect (del Pino Alemán et al. 2016; Alsina Ballester et al. 2016) shows no significant detection above $\sim 300\,\mathrm{G}$ in observations above ARs, except in one instance of particular interest: in NOAA 2372 we detected a field of 516 G at the $2.5\,\sigma$ level.

These results support the most recent theoretical understanding of the formation of the Mg II UV doublet, the validity of the current numerical modeling, and can be of great interest for the future analysis of spectropolarimetric observations in this important magnetic diagnostic of the solar chromosphere and TR.

We thank Robert M. Candey (NASA), Joseph B. Gurman (NASA), and Juan Fontenla, for stewarding legacy data and codes through the times and kindly helping us to locate them. We also thank the referee for comments and suggestions that helped us present more clearly the analysis of this unconventional, venerable data set. TdPA acknowledges funding from the European Research Council (ERC) under the European Union's Horizon 2020 research and innovation programme (grant agreement no. 742265). This material is based upon work supported by the National Center for Atmospheric Research, which is a major facility sponsored by the National Science Foundation under Cooperative Agreement No. 1852977.

APPENDIX

A. DATA ANALYSIS

The polarimetric modulation of the UVSP consisted of rotating the MgF_2 waveplate 16 times at 22.5° intervals. The (polarizing) grating of the spectrograph acted as the polarization analyzer. The observed modulated intensities can then be modeled as (Calvert et al. 1979)

$$S_j = I + p[a + b\cos(4\theta_j)]Q - p\,b\sin(4\theta_j)U + p\sin\delta\sin(2\theta_j)V\,, \qquad j = 0,\ldots,N-1\,, \tag{A1}$$

where $\theta_j = 2\pi j/N$ ($N = 16$ in our case) δ is the retardance of the waveplate, p is the polarization efficiency of the analyzer, and $a = (1+\cos\delta)/2$, $b = (1-\cos\delta)/2$ (at 2800 Å, $p = 0.72$, $\delta = 131°$, from laboratory measurements before launch; Henze & Stenflo 1987). The Stokes parameters I, Q, U, V of the incoming light are defined in the usual way (e.g., Landi Degl'Innocenti & Landolfi 2004). The

positive direction for Q was along the solar North-South line, which in our case was parallel to the limb.

In practice, there may be intensity drifts during the observation due to the finite duration of the modulation scheme ($\sim$ 5 minutes), which are not taken into account by Eq. (A1). We corrected for them by fitting a linear trend to the S_j series and substracting it, preserving the average. This produces typically small corrections with respect to Henze & Stenflo (1987).

The Stokes parameters at a given wavelength and spatial position are recoverd from the S_j through least-squares fitting or, equivalently, by discrete Fourier analysis (Figure 4),

$$S_j = \sum_{k=0}^{N-1} s_k \exp\left(2\pi \mathrm{i}\, \frac{jk}{N}\right) , \qquad s_k = \frac{1}{N} \sum_{i=0}^{N-1} S_j \exp\left(2\pi \mathrm{i}\, \frac{jk}{N}\right) . \tag{A2}$$

The s_k coefficients can be efficiently calculated by the Fast Fourier Transform algorithm (e.g., Press et al. 1992). Then[2] (cf. Eqs. (A1), (A2)),

$$I = s_0 - 2\,\frac{a}{b}\,\Re(s_4) , \qquad V = -\frac{2}{p \sin\delta}\,\Im(s_2) , \qquad Q = \frac{2}{pb}\,\Re(s_4) , \qquad U = \frac{2}{pb}\,\Im(s_4) . \tag{A3}$$

Note that only modes $s_{2,4}$ (and the *average* s_0) contribute to the signal.

The uncertainty of the modulated intensities at each wavelength is assumed to be Poissonian (i.e., $\sigma^2(S_j) \equiv \sigma^2(S) = \bar{S}$, where $\bar{S}$ is the average of the S_j. Then, by error propagation, $\sigma^2(s_0) = \sigma^2(S)/N$, $\sigma^2(\Re(s_k)) = \sigma^2(\Im(s_k)) = \sigma^2(S)/2N$ $(0 < k < 8)$, and therefore,

$$\sigma^2(I) \approx \frac{\sigma^2(S)}{N}, \qquad \sigma^2(V) = \frac{2}{(p \sin\delta)^2}\frac{\sigma^2(S)}{N}, \qquad \sigma^2(Q) = \sigma^2(U) = \frac{2}{(pb)^2}\frac{\sigma^2(S)}{N}. \tag{A4}$$

In some observations, a few pixels were lost due to telemetry glitches and only 14 or 15 S_j values were recovered in a given series; in those cases, a least-squares fitting was applied.

Random (white) noise introduces spurious power in all the modes—not just $k = 2$ and 4. Additionally, "slow" intensity drifts during the observation introduce more power at lower fequencies (Figure 4). Typically, we find that the noise from an average of modes $k = 3$ and 5-8, is consistent with the noise estimate given above assuming photon (Poisson) noise. In some cases, however, the power in mode $k = 1$ is clearly well above the average noise. We consider this as an indication of systematic artifacts in that observation, which likely affect also the mode $k = 2$; the circular polarization measurement in those cases is discarded, while the mode $k = 4$ (linear polarization) is typically protected from these drifts (see panels i-j in Figure 4).

Figure 5 shows the polarization observed at disk center with an observational setup identical to the limb observations of scattering polarization. We use the average at each Stokes parameter over all wavelengths and spatial positions as a calibration for the zero-polarization level—symmetry requires that a long enough integration over a wide area should show no polarization at any wavelength. Only Stokes Q needs to be significantly recalibrated.

REFERENCES

[2] Because the observed intensities are real ($S_j = S_j^*$, where * indicates complex conjugation), in our case $s_k = s_{16-k}^*$. Hence, $S_j = s_0 + 2\sum_{k=1}^{7}[\Re(s_k)\cos(\pi jk/8) - \Im(s_k)\sin(\pi jk/8)] + s_8$.

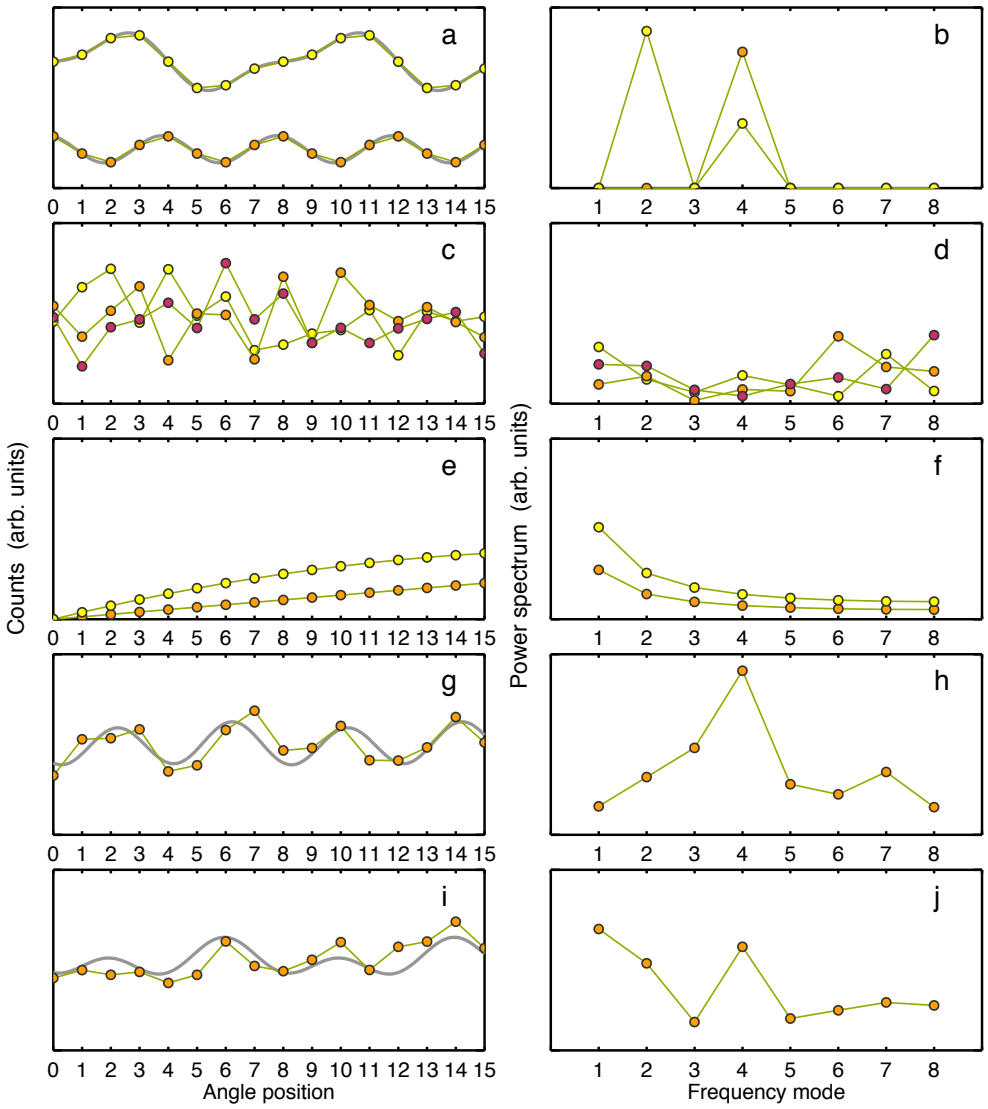


Figure 4. Modulated signals S_j in time space (left column), and corresponding power spectrum $|s_k|^2$ in Fourier space (right column); the redundant[2] Fourier modes 9-15 and the (much stronger) 0-th mode are not shown for clarity. a, b) Ideally, only modes 2 and 4, corresponding to circular and linear polarization, respectively, would be present in the signal. Here, two ideal cases are shown as illustration: a linearly polarized signal (orange) and an elliptically polarized (linear and circular components; yellow) signal. c, d) Random (white) noise introduces spurious power in all the modes. e, f) Intensity drifts—e.g., linear (orange), parabolic (yellow)—during the observation and other "slow" trend artifacts introduce more power at lower frequencies. g, h) Actual, observed noisy linearly polarized signal. Gray line: best fit reconstructed signal. i, j) Observed noisy signal with significant drift. Notice that the linear polarization mode ($k = 4$) is above the noise, but the circular polarization mode ($k = 2$) is below the mode $k = 1$, suggesting that it is also likely affected by drift. Panels g)-j) show raw, uncorrected (for intensity drift) data.

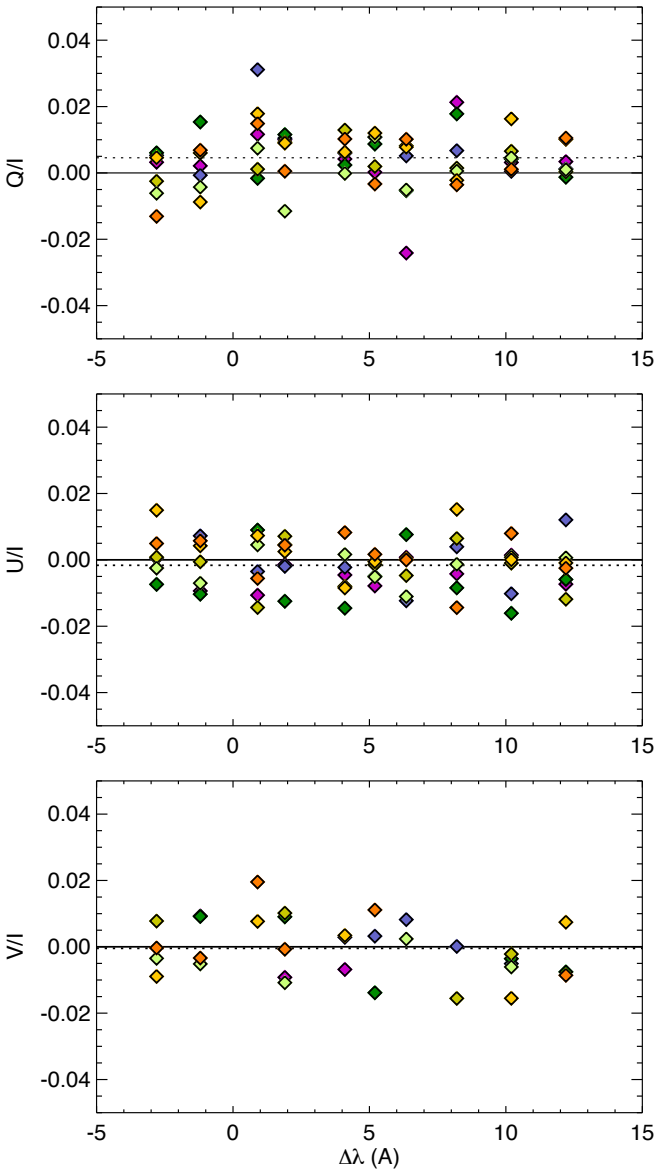


Figure 5. Polarization at disk center on October 30th, 1984 (01:36-02:24). Each color corresponds to a given spatial position (up to seven at a given wavelength). Between succesive wavelengths, ~ 5 min elapsed (scan proceeded from blue to red). Dotted lines show averages over all positions and wavelengths (wavelength scale centered at Mg II k-line).

Alsina Ballester, E., Belluzzi, L., & Trujillo Bueno, J. 2016, ApJL, 831, L15, doi: 10.3847/2041-8205/831/2/L15

Ambastha, A., & Bhatnagar, A. 1988, Journal of Astrophysics and Astronomy, 9, 137, doi: 10.1007/BF02715059

Auer, L. H., Rees, D. E., & Stenflo, J. O. 1980, A&A, 88, 302

Bohlin, J. D., Frost, K. J., Burr, P. T., Guha, A. K., & Withbroe, G. L. 1980, SoPh, 65, 5, doi: 10.1007/BF00151380

Calvert, J., Griner, D., Montenegro, J., et al. 1979, Optical Engineering, 18, 287, doi: 10.1117/12.7972368

Casini, R., del Pino Alemán, T., & Manso Sainz, R. 2017, ApJ, 848, 99, doi: 10.3847/1538-4357/aa8a73

del Pino Alemán, T., Casini, R., & Manso Sainz, R. 2016, ApJL, 830, L24, doi: 10.3847/2041-8205/830/2/L24

Fontenla, J. M., Avrett, E. H., & Loeser, R. 1993, ApJ, 406, 319, doi: 10.1086/172443

Giono, G., Ishikawa, R., Narukage, N., et al. 2017, SoPh, 292, 57, doi: 10.1007/s11207-017-1062-y

Hagyard, M. J., Teuber, D., West, E. A., et al. 1983, SoPh, 84, 13, doi: 10.1007/BF00157439

Henoux, J. C., Chambe, G., Sahal, S., et al. 1983, ApJ, 265, 1066, doi: 10.1086/160748

Henze, W., & Stenflo, J. O. 1987, SoPh, 111, 243, doi: 10.1007/BF00148517

Henze, Jr., W. 1993, Ultraviolet Spectrometer and Polarimeter (UVSP). Catalog of observations. Vol. 1. Experiments 1 - 30719 (February 1980 - April 1985).

Henze, Jr., W., Tandberg-Hanssen, E., Hagyard, M. J., et al. 1982, SoPh, 81, 231, doi: 10.1007/BF00151299

Jaynes, E. T. 2003, Probability Theory. The Logic of Science (Cambridge, UK: Cambridge University Press), 758

Krall, K. R., Smith, Jr., J. B., Hagyard, M. J., West, E. A., & Cummings, N. P. 1982, SoPh, 79, 59, doi: 10.1007/BF00146973

Landi Degl'Innocenti, E., & Landi Degl'Innocenti, M. 1972, SoPh, 27, 319, doi: 10.1007/BF00153104

Landi Degl'Innocenti, E., & Landolfi, M. 2004, Polarization in Spectral Lines (Dordrecht: Kluwer)

Machado, M. E., Somov, B. V., Rovira, M. G., & de Jager, C. 1983, SoPh, 85, 157, doi: 10.1007/BF00148266

Manso Sainz, R., del Pino Alemán, T., & Casini, R. 2017, ArXiv e-prints. https://arxiv.org/abs/1710.04155

Martínez González, M. J., Manso Sainz, R., Asensio Ramos, A., & Belluzzi, L. 2012, MNRAS, 419, 153, doi: 10.1111/j.1365-2966.2011.19681.x

Press, W. H., Teukolsky, S. A., Vetterling, W. T., & Flannery, B. P. 1992, Numerical recipes in FORTRAN. The art of scientific computing (Cambridge, UK: Cambridge University Press)

Rabin, D., Moore, R., & Hagyard, M. J. 1984, ApJ, 287, 404, doi: 10.1086/162699

Sawyer, C. 1982, Advances in Space Research, 2, 265, doi: 10.1016/0273-1177(82)90209-5

Strong, K. T., Saba, J. L. R., Haisch, B. M., & Schmelz, J. T., eds. 1999, The many faces of the sun : a summary of the results from NASA's Solar Maximum Mission

Tandberg-Hanssen, E., Cheng, C. C., Athay, R. G., et al. 1981, ApJL, 244, L127, doi: 10.1086/183496

Woodgate, B. E., Brandt, J. C., Kalet, M. W., et al. 1980, SoPh, 65, 73, doi: 10.1007/BF00151385